

Effect of Sn Doping on the Thermoelectric Properties of *n*-type Bi₂(Te,Se)₃ Alloys

JAE-UK LEE,^{1,3} DEUK-HEE LEE,¹ BEOMJIN KWON,¹ DOW-BIN HYUN,¹
SAHN NAHM,³ SEUNG-HYUB BAEK,^{1,2,4} and JIN-SANG KIM^{1,5}

1.—Future Convergence Research Division, Korea Institute of Science and Technology, Seoul 136-791, Republic of Korea. 2.—Department of Nanomaterials Science and Technology, Korea University of Science and Technology, Daejeon 305-333, Republic of Korea. 3.—Department of Materials Science and Engineering, Korea University, Seoul 136-713, Republic of Korea. 4.—e-mail: shbaek77@kist.re.kr. 5.—e-mail: jskim@kist.re.kr

In the present work, 0.01–0.05wt.% Sn-doped Bi₂(Te_{0.9}Se_{0.1})₃ alloys were prepared by mechanical deformation followed by hot pressing, and their thermoelectric properties were studied. We observed that the Sn element is a very effective dopant as an acceptor to control the carrier concentration in the *n*-type Bi₂(Te_{0.9}Se_{0.1})₃ alloys to optimize their thermoelectric property. The *n*-type carrier concentration can be controlled from $4.2 \times 10^{19}/\text{cm}^3$ to $2.4 \times 10^{19}/\text{cm}^3$ by 0.05wt.% Sn-doping. While the Seebeck coefficient and the electrical resistivity are both increased with doping, the power factor remains the same. Therefore, we found that the thermoelectric figure-of-merit becomes maximized at 0.75 when the thermal conductivity has a minimum value for the 0.03wt.% Sn-doped sample.

Key words: Bismuth telluride, thermoelectric, Sn doping, mechanical deformation, hot press

INTRODUCTION

The development of high-performance thermoelectric materials has been a challenging issue to realize thermoelectric modules for efficient power generation and eco-friendly refrigerating systems.^{1,2} The performance of thermoelectric materials is determined by the dimensionless figure-of-merit ($ZT = \alpha^2 \sigma T / \kappa$), where α is the Seebeck coefficient, σ is the electrical conductivity, and κ is the thermal conductivity, which is sum of the electronic (κ_{ele}) and lattice (κ_{lat}) thermal conductivities of the material.

Bismuth telluride (Bi₂Te₃) and their solid solutions with Sb₂Te₃ and Bi₂Se₃ are well known to have high thermoelectric performances at around room temperature. The Bi₂Te₃-based materials are traditionally fabricated by a single crystal growth method such as the zone melting and Bridgman methods.^{3–5} In cases of *n*-type thermoelectric materials, the single crystal has a better figure-of-

merit than the sintered material. Fleurial et al. reported an *n*-type single crystal of 36at.% Bi–64at.% Te prepared by the Bridgman method, obtaining a Seebeck coefficient of $-250 \mu\text{V/K}$, figure-of-merit of $2.9 \times 10^{-3}/\text{K}$ and carrier concentration of $2.0 \times 10^{19}/\text{cm}^3$.⁶ Despite excellent thermoelectric properties, single crystal materials have poor mechanical properties because of the weak van der Waals bonding between Te(1)-Te(1) layers in Te(1)-Bi-Te(2)-Bi-Te(1) and Te(1)-Bi-Te(2)-Bi-Te(1) along the *c* axis.^{7,8} The poor mechanical property makes it difficult to fabricate thermoelectric modules, and it is not appropriate for mass production.

In order to solve this problem, many researches have been conducted to improve the thermoelectric and mechanical properties by sintering techniques such as hot pressing and spark plasma sintering.^{9–12} Liu Xue-Dong et al. reported their work on *n*-type sintered Bi₂Te₃ with a Seebeck coefficient of $-130 \mu\text{V/K}$, figure of merit of $1.09 \times 10^{-3}/\text{K}$ and carrier concentration of $6.44 \times 10^{19}/\text{cm}^3$ by using mechanical alloying and spark plasma sintering at room temperature.¹³ Lee et al. reported *n*-type

sintered Bi₂Te_{2.85}Se_{0.15} prepared by melting and grinding with subsequent hot pressing, obtaining a Seebeck coefficient of $-140 \mu\text{V/K}$, figure-of-merit of $1.9 \times 10^{-3}/\text{K}$, and carrier concentration of $7.37 \times 10^{19}/\text{cm}^3$ at 373 K.¹⁴

However, since the carrier concentration of *n*-type sintered materials has to be higher than that of *n*-type single crystal due to the large density of defects such as Te_{Bi}, and V_{Te} which play a role in the generation of electrons,¹⁵ the sintered materials have a lower Seebeck coefficient than the single crystal. As a result, the figure-of-merit of sintered materials is lower than that of the single crystal. The Seebeck coefficient is inversely proportional to the carrier concentration while the electrical conductivity and thermal conductivity are proportional to the carrier concentration. Therefore, the optimization of carrier concentration will be a promising approach to improve the figure-of-merit of *n*-type thermoelectric sintered materials.

In the present study, we describe the thermoelectric and electrical properties of Sn-doped Bi₂(Te_{0.9}Se_{0.1})₃ alloys. The Sn is used as an acceptor in Bi₂(Te_{0.9}Se_{0.1})₃ alloys to reduce the carrier concentration. Sn-doped Bi₂(Te_{0.9}Se_{0.1})₃ alloys were prepared by mechanical deformation,^{16,17} and followed hot pressing. In general, the sintered Bi-Te-based materials are fabricated by powder processing such as melting/grinding and mechanical alloying. However, the surface oxidation of the powder can potentially occur during such powder processing.^{8,9,18} As the oxygen acts as a donor in Bi-Te-based materials, this fabrication method may not be appropriate for our doping study.⁹ Therefore, we used a different technique using mechanical deformation to suppress the oxygen doping effects in this work. The detailed procedure and working mechanism of this process is described in Ref. 16.

EXPERIMENTAL PROCEDURES

n-type Bi₂(Te_{0.9}Se_{0.1})₃ + *x*wt.% Sn (*x* = 0, 0.01, 0.03, 0.05) was prepared using Bi(99.997%), Te(99.99999%), Se(99.999%), and Sn(99.9%) granules as starting materials. The materials were weighed according to the chemical formula, melted in an evacuated quartz tube by a rocking furnace at 750°C for about 5 h, and then rapidly cooled to room temperature to produce a homogeneous ingot. Specimens were cut from the ingot into rectangular parallelepipeds (5 mm × 5 mm × 12 mm) and mechanically deformed by cold pressing at 700 MPa using a steel mold. After the first mechanical deformation, the specimen was removed from the steel mold and repressed in the direction perpendicular to the previous pressing direction. The mechanical deformation process was carried out 10 times. The deformed specimens were loaded into a graphite mold, and sintered by hot pressing at 500°C under 40 MPa for 1 h in vacuum. The graphite mold and punch were coated with BN

particles in order to reduce friction during the removal of the specimens from the graphite mold.

X-ray diffraction (XRD) patterns of the hot-pressed specimens were obtained in θ - 2θ mode using an x-ray diffractometer (D8 Discover; Bruker AXS Korea, Korea) with Cu K α radiation. The Seebeck coefficient was measured by commercial equipment (TEP600; Seepel, Korea). After measuring the Seebeck coefficient, the hot-pressed specimens were cut into rectangular parallelepipeds (1.5 mm × 1.5 mm × 11.5 mm) and thin rectangular parallelepipeds (thickness of less than 150 μm) by an electro-discharge machine for Harman¹⁹ and Hall measurements, respectively. Electrical conductivity was measured by the four-point probe method. For measuring the dimensionless figure-of-merit, the Harman method was conducted. The thermal conductivity was calculated by $\kappa = \alpha^2 \sigma / Z$. The carrier concentration and mobility were measured by Hall measurement (HMS3000; Ecopia, Korea), and a magnetic field of 0.55 T and electrical current of 15 mA were applied.

RESULTS AND DISCUSSION

Figure 1 shows the XRD patterns of the hot-pressed Bi₂(Te_{0.9}Se_{0.1})₃ + *x*wt.% Sn, obtained from the sample normal vector parallel to the final pressing direction. The peak intensities were normalized to the (015) diffraction peak. The diffraction peaks are well matched with the standard diffraction pattern of Bi₂(Te_{0.9}Se_{0.1})₃ (PDF # 50-0954), which means that none of the specimens have a secondary phase. The Sn dopant had no significant effect on the diffraction patterns because its amount was too small.

The carrier concentration and mobility of Bi₂(Te_{0.9}Se_{0.1})₃ alloys as a function of the amount of Sn are shown in Fig. 2. With increasing the amount of Sn, the carrier concentration is decreased from

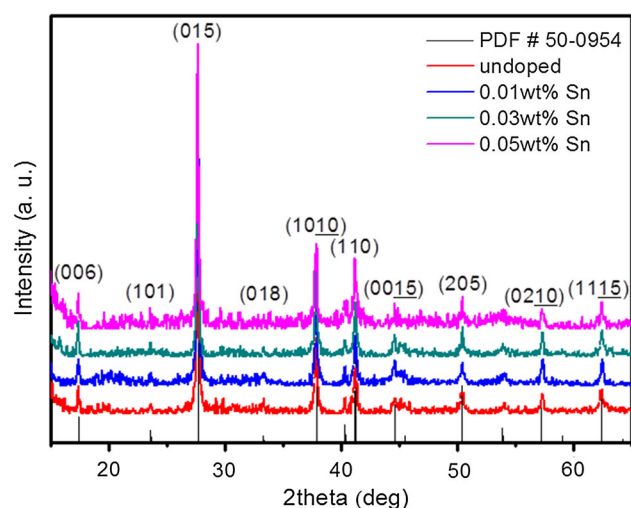


Fig. 1. X-ray diffraction patterns of Bi₂(Te_{0.9}Se_{0.1})₃ + 0, 0.01, 0.03, 0.05wt.% Sn alloys.

$4.2 \times 10^{19}/\text{cm}^3$ to $2.4 \times 10^{19}/\text{cm}^3$, since the Sn dopant acts as an acceptor by occupying the Bi site. The Sn dopant can easily occupy the Bi site because of small differences in electronegativity between Bi (2.02) and Sn (1.96). The following equation describes the ideal case of *n*-type Bi-Te-based materials.²⁰

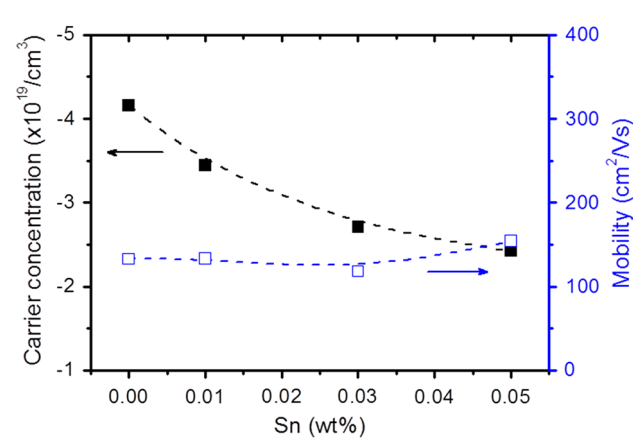
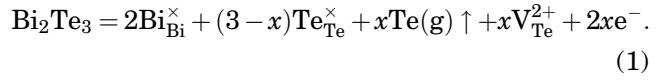
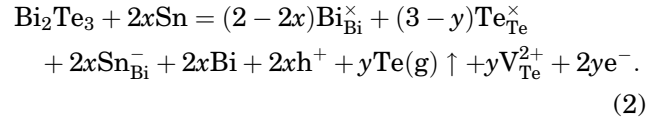


Fig. 2. Carrier concentration and mobility of $\text{Bi}_2(\text{Te}_{0.9}\text{Se}_{0.1})_3$ alloys as a function of the amount of Sn.



Here, the addition of Sn in *n*-type Bi-Te-based materials can be expressed as follows:



Each Sn atom occupied in the Bi site makes two holes, compensating two electron carriers, and hence it reduces *n*-type carrier concentration. The mobility is fractionally increased due to the effect of the reduced carrier concentration.

Figure 3 shows the variation of the Seebeck coefficient, electrical conductivity, power factor, and thermal conductivity for Sn-doped $\text{Bi}_2(\text{Te}_{0.9}\text{Se}_{0.1})_3$ as a function of the Sn amount. The Seebeck coefficient of all specimens had a negative value, which indicates that the majority of the carriers are electrons. With increasing the amount of Sn from 0wt.% to 0.05wt.%, the Seebeck coefficient was increased from $-153.2 \mu\text{V}/\text{K}$ to $-230.6 \mu\text{V}/\text{K}$ due to the reduced carrier concentration, as shown in Fig. 3a. The relationship between the Seebeck coefficient

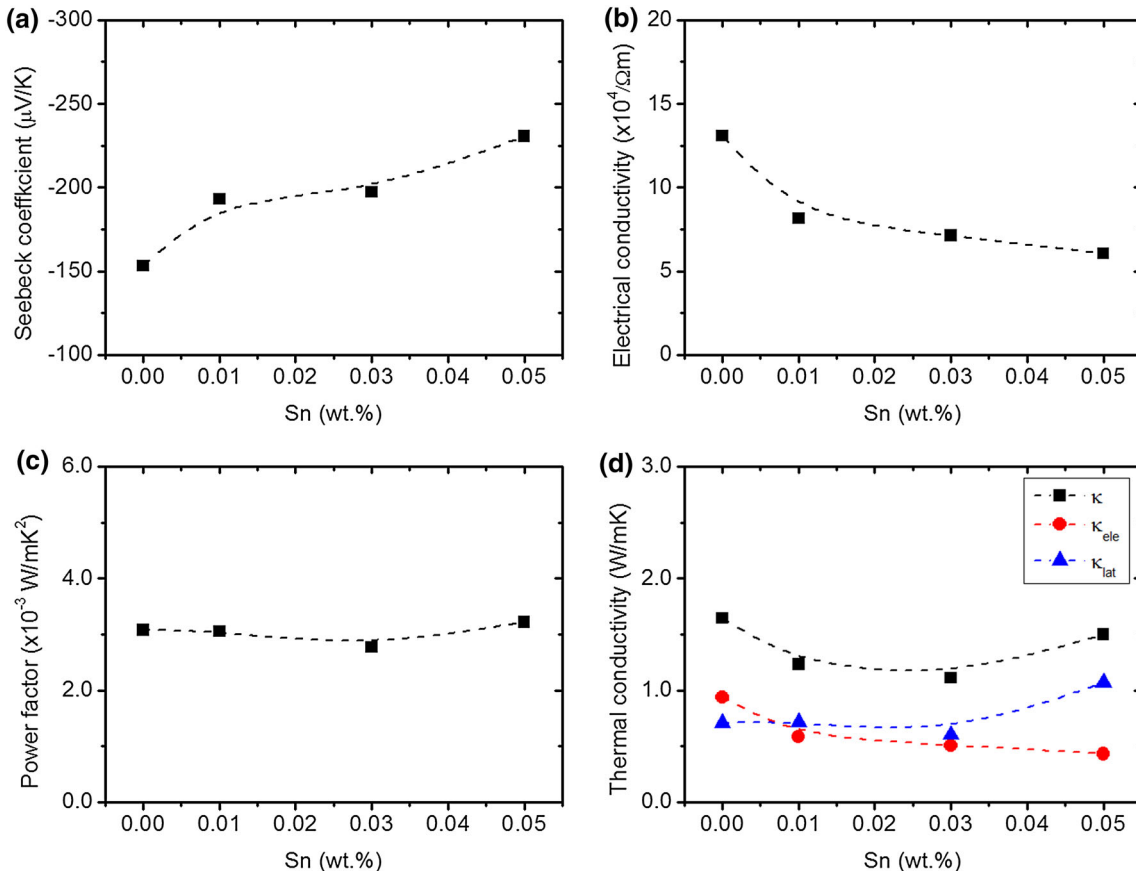


Fig. 3. (a) Seebeck coefficient, (b) electrical conductivity, (c) power factor, and (d) thermal conductivity of $\text{Bi}_2(\text{Te}_{0.9}\text{Se}_{0.1})_3$ alloys as a function of the amount of Sn.

and the carrier concentration can be expressed as follows²¹:

$$\alpha = \frac{8\pi^2 k_B^2}{3eh^2} m^* T \left(\frac{\pi}{3n} \right)^{\frac{2}{3}}, \quad (3)$$

where π , k_B , e , h , m^* , T , and n are the Peltier coefficient, Boltzmann constant, electron charge, Planck constant, effective mass, absolute temperature, and carrier concentration, respectively.

The electrical conductivity can be expressed as the following relationship²¹:

$$\sigma = ne\mu, \quad (4)$$

where μ is the mobility.

The electrical conductivity is related to the carrier concentration and mobility. According to Fig. 2, as the amount of Sn dopant increases from 0wt.% to 0.05wt.%, the carrier concentration of the $\text{Bi}_2(\text{Te}_{0.9}\text{Se}_{0.1})_3$ decreases by 41.8%. On the other hand, the mobility increases by 15.9%. Consequently, the electrical conductivity decreases from $13.1 \times 10^4/\Omega\text{m}$ to $6.06 \times 10^4/\Omega\text{m}$ with Sn doping (Fig. 3b).

The power factor was calculated from the measured Seebeck coefficient and electrical conductivity by the equation $PF = \alpha^2 \sigma$. As shown in Fig. 3c, the power factor has almost a constant value regardless of the amount of Sn. Although the electrical conductivity was

decreased with the reduced carrier concentration, the increased Seebeck coefficient compensated for power factor.

The thermal conductivity is defined as the contribution of electronic thermal conductivity and lattice thermal conductivity. So, the thermal conductivity is given by¹⁷:

$$\kappa = \kappa_{\text{ele}} + \kappa_{\text{lat}} = ne\mu LT + \kappa_{\text{lat}}, \quad (5)$$

where κ_{ele} is the electronic thermal conductivity, κ_{lat} is the lattice thermal conductivity, and L is the Lorentz number.

The electronic thermal conductivity can be calculated by using the Wiedemann–Franz law ($\kappa_{\text{ele}} = ne\mu LT$), where $L = 2.45 \times 10^{-8} \text{ W } \Omega/\text{K}^2$.²¹ With increasing the amount of Sn, the electronic thermal conductivity was decreased due to the reduced carrier concentration. While the electronic thermal conductivity was decreased, the lattice thermal conductivity was increased due to influence of the Sn atoms, which cause lattice distortion of the crystal structure. As a result, the total thermal conductivity of up to the amount of 0.03wt.% Sn was decreased, but thereafter was increased, as shown in Fig. 3d.

Figure 4 shows the variation of the dimensionless figure-of-merit with the amount of Sn. Undoped $\text{Bi}_2(\text{Te}_{0.9}\text{Se}_{0.1})_3$ had a relatively low ZT of 0.56. The ZT of up to the amount of 0.03wt.% Sn was increased due to the enhanced Seebeck coefficient and reduced thermal conductivity, despite the decreased electrical conductivity. On the other hand, in spite of the enhanced Seebeck coefficient, the ZT of 0.05wt.% Sn-doped specimen was reduced due to the decreased electrical conductivity and increased thermal conductivity, compared to the 0.03wt.% Sn-doped specimen. The maximum ZT of 0.75 was obtained for 0.03wt.% Sn-doped $\text{Bi}_2(\text{Te}_{0.9}\text{Se}_{0.1})_3$. The effect of Sn doping on the thermoelectric properties of n -type $\text{Bi}_2(\text{Te}_{0.9}\text{Se}_{0.1})_3$ is summarized in Table I.

CONCLUSIONS

In this study, the effect of Sn-doping on the thermoelectric properties was investigated. In order to optimize the carrier concentration, Sn-doped n -type sintered $\text{Bi}_2(\text{Te}_{0.9}\text{Se}_{0.1})_3$ alloys were fabricated

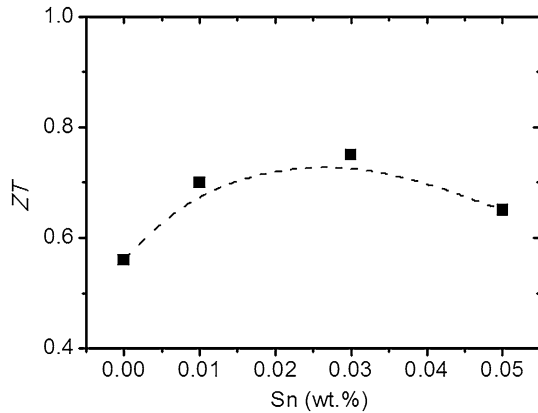


Fig. 4. Variation of dimensionless figure-of-merit ZT of $\text{Bi}_2(\text{Te}_{0.9}\text{Se}_{0.1})_3$ alloys as a function of the amount of Sn.

Table I. Summarized thermoelectric properties of Sn-doped $\text{Bi}_2(\text{Te}_{0.9}\text{Se}_{0.1})_3$

Specimen	Carrier concentration ($\times 10^{19}/\text{cm}^3$)	Seebeck coefficient ($\mu\text{V}/\text{K}$)	Electrical conductivity ($\times 10^4/\Omega\text{m}$)	Thermal conductivity (W/mK)			Power factor ($\times 10^{-3} \text{ W}/\text{mK}^2$)	ZT
				κ_{ele}	κ_{lat}	κ_{tot}		
Undoped	4.2	-153	13.1	0.94	0.71	1.65	3.08	0.56
0.01wt.% Sn	3.4	-193	8.2	0.58	0.72	1.30	3.05	0.70
0.03wt.% Sn	2.7	-197	7.1	0.51	0.60	1.11	2.77	0.75
0.05wt.% Sn	2.4	-230	6.1	0.43	1.07	1.50	3.22	0.65

by mechanical deformation followed by hot pressing at 500°C. The XRD peaks were well matched with the standard diffraction pattern without any secondary phases. The carrier concentration in the *n*-type sintered Bi₂(Te_{0.9}Se_{0.1})₃ alloys was reduced by doping Sn as an acceptor. The carrier density was decreased with the amount of Sn dopant, leading to the increase of the Seebeck coefficient and the decrease of the electrical conductivity. We observed that the power factor was almost the same regardless of the Sn content. The thermal conductivity has a minimum value when 0.03wt.% Sn was added. Therefore, we found that the thermoelectric property of *n*-type Bi₂(Te_{0.9}Se_{0.1})₃ has a maximum value of 0.75 when 0.03wt.% Sn acceptor dopant is added.

ACKNOWLEDGEMENT

J.-U.L. and D.-H.L. contributed equally to this work. This research was supported by the Technology Innovation Program (10046673) funded by the Ministry of Trade, Industry & Energy (MI, Korea), and KIST-UNIST partnership program through 2V03290.

REFERENCES

1. B.C. Sales, *Science* 295, 1248 (2002).
2. L.E. Bell, *Science* 321, 1457 (2008).
3. J. Jiang, L. Chen, Q. Yao, S. Bai, and Q. Wang, *Mater. Chem. Phys.* 92, 39 (2005).
4. D.B. Hyun, J.S. Hwang, B.C. You, T.S. Oh, and C.W. Hwang, *J. Mater. Sci.* 33, 5595 (1998).
5. M.H. Ettenberg, J.R. Maddux, P.J. Taylor, W.A. Jesser, and F.D. Rosi, *J. Cryst. Growth* 179, 495 (1997).
6. J.P. Fleurial, L. Gailliard, R. Triboulet, H. Scherrer, and S. Scherrer, *J. Phys. Chem. Solids* 49, 1237 (1988).
7. J.R. Daabble and C.H.L. Goodman, *J. Phys. Chem. Solids* 5, 142 (1958).
8. D.H. Lee, J.U. Lee, S.J. Jung, S.H. Baek, J.H. Kim, D.I. Kim, D.B. Hyun, and J.S. Kim, *J. Electron. Mater.* 43, 2255 (2014).
9. T.S. Oh, D.B. Hyun, and N.V. Kolomoets, *Scr. Mater.* 42, 849 (2000).
10. X.A. Fan, J.Y. Yang, W. Zhu, H.S. Yun, R.G. Chen, S.Q. Bao, and X.K. Duan, *J. Alloys Compd.* 420, 256 (2006).
11. J.Y. Yang, T. Aizawa, A. Yamamoto, and T. Ohta, *J. Alloys Compd.* 312, 326 (2000).
12. X.A. Fan, G.Q. Li, W. Zhong, X.K. Duan, and J.Y. Yang, *Integr. Ferroelectr.* 1128, 1 (2011).
13. L.X. Dong and Y.H. Park, *Mater. Trans.* 43, 681 (2002).
14. G.E. Lee, I.H. Kim, Y.S. Lim, W.S. Seo, B.J. Choi, and C.W. Hwang, *J. Electron. Mater.* 43, 1650 (2014).
15. P. Pecheur and G. Toussaint, *J. Phys. Chem. Solids* 55, 327 (1994).
16. S.J. Jung, J.H. Kim, D.I. Kim, S.K. Kim, H.H. Park, J.S. Kim, D.B. Hyun, and S.H. Baek, *Phys. Chem. Chem. Phys.* 16, 3529 (2014).
17. S.J. Jung, S.K. Kim, H.H. Park, D.B. Hyun, S.H. Baek, and J.S. Kim, *J. Nanomater.* 2013, 6 (2013).
18. D.M. Lee, C.H. Lim, D.C. Cho, Y.S. Lee, and C.H. Lee, *J. Electron. Mater.* 35, 360 (2006).
19. T.C. Harman, J.H. Cahn, and M.J. Logan, *J. Appl. Phys.* 30, 1351 (1959).
20. W.S. Liu, Q. Zhang, Y. Lan, S. Chen, X. Yan, Q. Zhang, H. Wang, D. Wang, G. Chen, and Z. Ren, *Adv. Energy Mater.* 1, 577 (2011).
21. G.J. Snyder and E.S. Toberer, *Nat. Mater.* 7, 105 (2008).